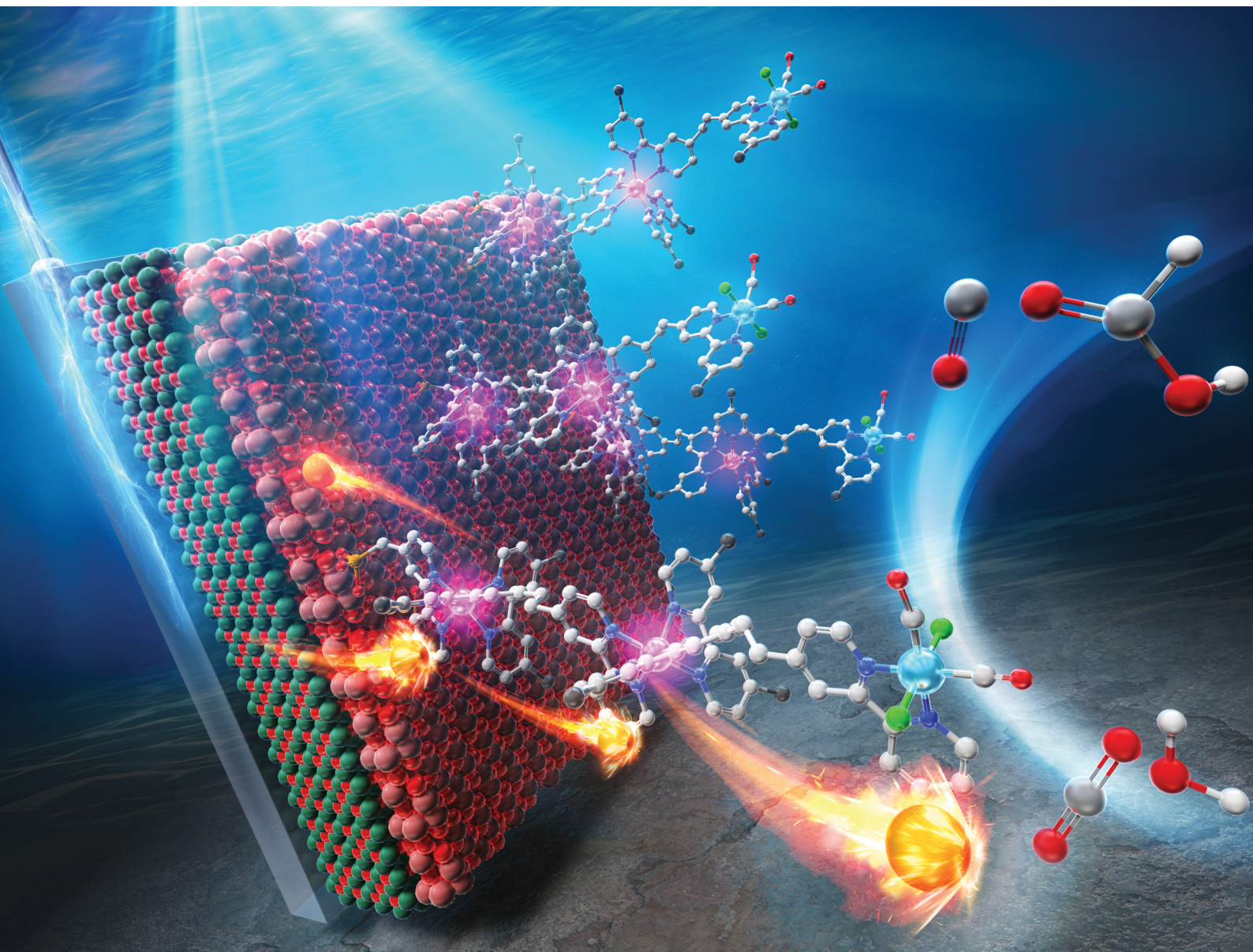


ChemComm

Chemical Communications

rsc.li/chemcomm



ISSN 1359-7345

COMMUNICATION

Ken Onda, Osamu Ishitani, Kazuhiko Maeda *et al.*
Introducing an insulating alumina layer into a molecular
photocathode to improve CO₂ reduction activity


 Cite this: *Chem. Commun.*, 2026, 62, 8169

 Received 27th January 2026,
 Accepted 27th March 2026

DOI: 10.1039/d6cc00558f

rsc.li/chemcomm

Introducing an insulating alumina layer into a molecular photocathode to improve CO₂ reduction activity

 Yu Takagi,^a Masaya Yara,^b Toshiya Tanaka,^a Jo Onodera,^a Minato Tanaka,^a Megumi Okazaki,^{ib} Kiyoshi Miyata,^b Ken Onda,^{ib}*^b Osamu Ishitani,^{ib}*^c and Kazuhiko Maeda,^{ib}*^{ad}

Interfacial engineering with an Al₂O₃ overlayer enhances visible-light-driven CO₂ reduction on p-type NiO photocathodes incorporating Ru(II)-based photosensitizing molecular units. Operando transient absorption spectroscopy reveals that Al₂O₃ suppresses charge recombination between NiO and the photosensitizer unit, prolonging carrier lifetimes and improving catalytic efficiency.

Following the establishment of the spectral sensitization concept by Gerischer,¹ hybrids composed of light-absorbing molecules (*i.e.*, photosensitizers) and semiconductors have long served as fundamental building blocks for dye-sensitized solar cells (DSSCs)² and photocatalytic systems.^{3,4} The direction of interfacial electron transfer in such hybrid systems is governed by the conduction type of the semiconductor. For instance, in systems employing n-type TiO₂ in combination with Ru(II)-based photosensitizers, upward band bending at the n-TiO₂/solution interface facilitates electron injection from the photoexcited sensitizer into the semiconductor. By contrast, when a p-type semiconductor such as NiO is used, electron transfer from the semiconductor to the photoexcited photosensitizer becomes feasible because of downward band bending, enabling the construction of photoelectrochemical cells for water splitting⁵ and CO₂ reduction.^{6,7}

A representative example is a photocathode composed of a Ru(II)–Re(I) binuclear complex (**RuRe**) immobilized on NiO, which selectively reduces CO₂ to CO (Scheme S1 and Fig. S1).⁶ **RuRe** and its analogues were originally developed as homogeneous

photocatalysts for visible-light CO₂ reduction.⁸ Upon photoexcitation of **RuRe** *via* singlet metal-to-ligand charge transfer, the excited Ru unit accepts an electron from the p-type NiO substrate to generate a one-electron-reduced species. This electron is subsequently transferred to the catalytically active Re center. Repetition of this sequence enables the accumulation of two electrons at the Re site, thereby driving the two-electron reduction of CO₂ to CO. However, competitive back electron transfer from the reduced Ru or Re species to NiO can occur, leading to diminished CO₂ reduction efficiency. Consequently, precise interfacial engineering that retards charge recombination while preserving efficient electron injection is a key requirement for high-performance molecule/semiconductor hybrid photocathodes.

In n-TiO₂-based DSSCs, charge recombination between the photosensitizer and the semiconductor can be effectively suppressed by conformally coating TiO₂ with a thin metal oxide overlayer possessing a higher conduction band edge.⁹ Such overlayers increase the physical separation at the photosensitizer/TiO₂ interface, thereby retarding back electron transfer.¹⁰ Although increasing this separation can also impede forward electron injection, the much slower kinetics of back electron transfer enable selective suppression of recombination without compromising the overall photofunctional performance.¹¹ Further improvements have been achieved by precisely controlling the overlayer thickness using surface engineering techniques such as atomic layer deposition.^{12,13}

By contrast, analogous surface modification strategies for p-type semiconductors remain scarcely explored. Only four examples of metal-oxide coatings on p-type semiconductor surfaces have thus far been reported.^{14–17} Among these, three involve p-NiO-based DSSCs; the sole example of the strategy being applied to a photocathode is the water-splitting system reported by Ji *et al.*¹⁷ Notably, the influence of the oxide overlayer precursor concentration and its effect on carrier dynamics in p-type semiconductor/molecular photocatalyst hybrid systems have not yet been investigated.

^a Department of Chemistry, School of Science, Institute of Science Tokyo, 2-12-1-NE-2 Ookayama, Meguro-ku, Tokyo 152-8550, Japan.

E-mail: maeda@chem.sci.isct.ac.jp

^b Department of Chemistry, Faculty of Science, Kyushu University, 744 Motoooka, Nishi-ku, Fukuoka 819-0395, Japan. E-mail: konda@chem.kyushu-univ.jp

^c Department of Chemistry, Graduate School of Advanced Science and Engineering, Hiroshima University, 1-3-1 Kagamiyama, Higashi-Hiroshima, Hiroshima 739-8526, Japan. E-mail: iosamu@hiroshima-u.ac.jp

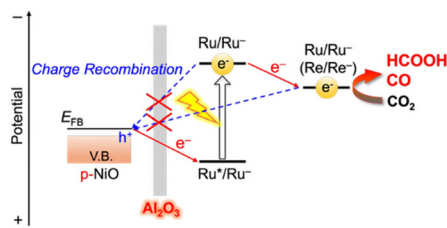
^d Research Center for Autonomous Systems Materialogy (ASMat), Institute of Science Tokyo, 4259 Nagatsuta-cho, Midori-ku, Yokohama, Kanagawa 226-8501, Japan



Herein, we report Al₂O₃-coated NiO electrodes further functionalized with either a Ru(II)–Re(I) binuclear complex (**RuRe**) or polymerized Ru complexes (poly-**RuRu'**) as hybrid photocathodes for visible-light-driven CO₂ reduction. The Al₂O₃ overlayer is introduced to suppress interfacial charge recombination (Scheme 1), and its effect on charge carrier dynamics is systematically examined using *operando* transient absorption spectroscopy.

NiO electrodes were fabricated on fluorine-doped tin oxide (FTO) substrates using a squeegee method, as reported previously.¹⁸ The formation of NiO on FTO was confirmed by X-ray photoelectron spectroscopy (XPS) and X-ray diffraction (XRD) measurements (Fig. S2). The as-prepared NiO electrodes were then immersed in 2-propanol solutions containing different concentrations (*C*) of aluminum tri-*sec*-butoxide, followed by heat treatment⁹ to afford Al₂O₃-modified NiO electrodes (denoted as *C*-Al₂O₃/NiO). Full experimental details are described in the SI.

Cross-sectional scanning electron microscopy combined with energy-dispersive X-ray spectrometry (SEM–EDS) of the 0.15 mM-Al₂O₃/NiO electrode revealed a NiO nanoparticle layer with particle diameters of approximately 20 nm and a thickness of ~600 nm deposited onto the FTO substrate (Fig. 1a). Although Al species could not be detected by EDS because of their low absolute concentration (Fig. S3), depth profiling by time-of-flight secondary-ion mass spectrometry (TOF-SIMS) clearly showed Al⁺ signals throughout the NiO layer (Fig. 1b). The Al⁺ signals persisted until the appearance of Sn⁺ signals originating from the FTO substrate, indicating that Al species were distributed across the entire NiO nanoparticle layer. The presence of Al₂O₃ was further supported by Fourier transform infrared (FT-IR) spectra (Fig. S4), which showed Al–O symmetric stretching vibration bands at the <1000 cm⁻¹ region.^{19,20} By contrast, XRD analysis did not show diffraction peaks attributable to crystalline Al-containing phases; only reflections from NiO and the FTO substrate were observed (Fig. S2a). This result suggests that the Al₂O₃ deposited onto NiO is amorphous. XPS measurements indicated that the electronic state of NiO remains essentially unchanged after Al₂O₃ modification, suggesting that the interaction between Al₂O₃ and NiO is weak. The XPS results also indicated that direct detection of Al signals was difficult because the Al 2s region overlaps with that of Ni 2p (Fig. S2b).



Scheme 1 Introduction of an insulating Al₂O₃ layer onto NiO further functionalized with a binuclear Ru(II)–Re(I) complex (**RuRe**) or a polymerized Ru(II) complex (poly-**RuRu'**).

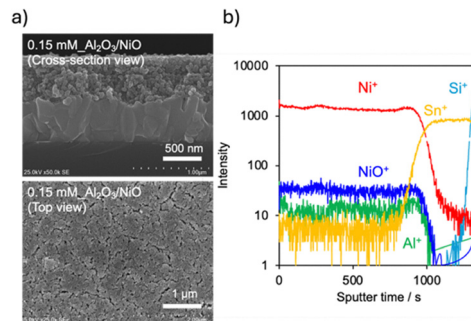


Fig. 1 (a) SEM images and (b) TOF-SIMS spectra representing the distribution of elements in the depth direction for 0.15 mM-Al₂O₃/NiO.

The surface morphologies of NiO, 0.15 mM-Al₂O₃/NiO, and 150 mM-Al₂O₃/NiO electrodes were examined by atomic force microscopy (AFM) (Fig. S5). The 0.15 mM-Al₂O₃/NiO electrode exhibited spherical particles similar to those of the unmodified NiO electrode, accompanied by a slight increase in particle size, suggesting the formation of a thin Al₂O₃ overlayer with an estimated thickness of ~4 nm. By contrast, the 150 mM-Al₂O₃/NiO electrode showed substantial interparticle connections, obscuring the original spherical morphology of the NiO. This observation indicates that the deposition of excessive Al₂O₃ fills the interparticle voids of the NiO layer. Thus, increasing the precursor concentration enables systematic control over the thickness of the Al₂O₃ overlayer, consistent with previous observations of Al₂O₃-modified TiO₂ electrodes for dye-sensitized solar cells.⁹

To evaluate the photoelectrochemical performance as a function of the Al₂O₃ precursor concentration, **RuRe** was first immobilized onto the *C*-Al₂O₃/NiO electrodes (**RuRe/C**-Al₂O₃/NiO). **RuRe/C**-Al₂O₃/NiO can be prepared using a simple adsorption method, which is convenient for optimization purposes. Incident photon-to-current conversion efficiencies (IPCEs) were measured at –0.7 V vs. Ag/AgCl under monochromatic irradiation at 460 nm. During photoelectrochemical CO₂ reduction using **RuRe**/NiO with cathodic polarization, electrons are supplied from the counter electrode and cathodic polarization shifts the Fermi level of NiO toward more negative potentials. This shift results in increased band bending at the NiO/solution interface, thereby enhancing electron injection from the semiconductor into the molecular photocatalyst. As shown in Fig. S6, the IPCE increased with increasing *C*, reached a maximum at *C* = 1.5 mM, and decreased at higher concentrations. Under the optimized conditions, the IPCE was enhanced by a factor of approximately two compared with that of the unmodified NiO electrode. Although the adsorption amount of **RuRe** slightly increased because of the enhanced surface area resulting from Al₂O₃ modification, no correlation was observed between the amount of adsorbed **RuRe** and the IPCEs (Table S1).

RuRe/NiO photocathodes have been reported to deactivate within 5 h because of detachment of the **RuRe** complex from the semiconductor surface, whereas poly-**RuRu'**/NiO electrodes exhibit substantially improved long-term stability.²¹ On the basis of this enhanced durability, we chose poly-**RuRu'**/NiO as



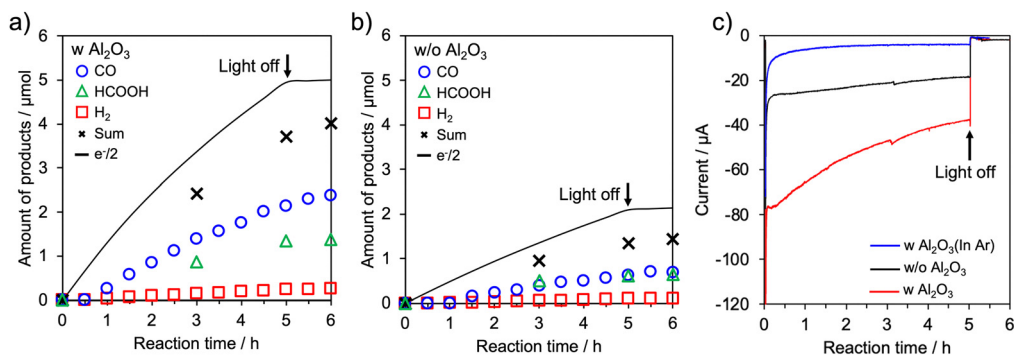


Fig. 2 Time courses of CO, HCOOH, and H₂ evolution of (a) poly-RuRu'/0.15 mM Al₂O₃/NiO (w Al₂O₃) and (b) poly-RuRu'/NiO (w/o Al₂O₃). (c) Current-time curves for poly-RuRu'/0.15 mM Al₂O₃/NiO (w Al₂O₃), and poly-RuRu'/NiO (w/o Al₂O₃) under visible-light irradiation (32 mW cm⁻², 460 nm < λ < 650 nm). The measurements were conducted in a 50 mM aqueous NaHCO₃ solution under a CO₂ or an Ar atmosphere (pH 6.6) and under an electrochemical bias of -0.7 V vs. Ag/AgCl. Irradiation area, 2.5 cm².

a more suitable platform for evaluating the effect of Al₂O₃ surface modification. As previously noted, molecular photocatalysts were immobilized onto the NiO surface *via* electrochemical polymerization (Fig. S7 and S8). The loading amount of electrochemically active poly-RuRu' on NiO was estimated from the Ru³⁺/Ru²⁺ redox peaks observed in cyclic voltammograms to be approximately 18 nmol, irrespective of Al₂O₃ modification (Fig. S9).

Photoelectrochemical CO₂ reduction was carried out using poly-RuRu'/0.15 mM Al₂O₃/NiO and poly-RuRu'/NiO electrodes at -0.7 V vs. Ag/AgCl in an aqueous NaHCO₃ solution under a CO₂ atmosphere. The electrodes were irradiated with visible light (460 nm < λ < 650 nm) using a 300 W Xe lamp equipped with a cutoff filter. CO and HCOOH were identified as the main reduction products, accompanied by a small amount of H₂ (Fig. 2). Notably, the amounts of CO and HCOOH produced were increased by approximately threefold upon Al₂O₃ modification. Consistent with this enhancement, the photocurrent density of the poly-RuRu'/0.15 mM Al₂O₃/NiO electrode under irradiation was higher than that of the unmodified poly-RuRu'/NiO electrode. By contrast, under an Ar atmosphere, substantially lower photocurrents were observed, confirming that the observed photocurrent enhancement originates from CO₂ reduction. The action spectrum recorded at various excitation wavelengths was similar to the absorption spectrum of poly-RuRu'. Higher IPCEs were obtained at all wavelengths compared with the IPCEs of the unmodified electrode, with a maximum of 2.9 ± 0.5% observed at 460 nm (Fig. S10).

These results clearly demonstrate that the CO₂ reduction performance of the hybrid photocathode can be enhanced by inserting an Al₂O₃ interlayer between the molecular photocatalyst and NiO. Although the flat-band potential (E_{FB}) of a p-type semiconductor is known to influence the efficiency of electron transfer to an adsorbed photosensitizer,²² the E_{FB} of NiO was found to remain essentially unchanged after the Al₂O₃ modification (Fig. S11). This result indicates that the energetics of electron injection from the NiO to the molecular photocatalyst is not altered by the Al₂O₃ layer. Therefore, the observed enhancement in CO₂ reduction activity is attributed to changes in charge carrier dynamics at the semiconductor/molecular interface induced by the Al₂O₃ modification.

To gain insight into the role of the Al₂O₃ interlayer, we analyzed the poly-RuRu'/0.15 mM Al₂O₃/NiO and poly-RuRu'/NiO photocathodes using *operando* transient absorption spectroscopy. Charge carrier dynamics under operating conditions were monitored at -0.7 V vs. Ag/AgCl in a CO₂-saturated aqueous solution using 420 nm laser excitation. Upon pulsed photoexcitation, bleaching of the ground state was observed (Fig. S12). The bleaching signals, monitored at 465–470 nm for both electrodes, gradually recovered within several hundred nanoseconds (Fig. 3). This recovery is attributed to charge recombination between the one-electron-reduced photosensitizing unit and holes in the NiO and/or electron transfer from the photosensitizer to the catalytic unit. Notably, the recovery of the bleaching signal was delayed upon Al₂O₃ modification, giving double exponential bleaching recovery rate constants of $k_1 = 3.8 \times 10^8$ and $k_2 = 2.7 \times 10^7$ s⁻¹, which were smaller than those obtained without Al₂O₃ modification ($k_1 = 5.6 \times 10^8$ and $k_2 = 6.7 \times 10^7$ s⁻¹) (Fig. S12c). This delayed recovery clearly indicates suppression of back electron transfer between the semiconductor and the molecular photocatalyst by the Al₂O₃ interlayer. The suppressed back electron transfer upon Al₂O₃ modification was also supported by electrochemical impedance spectroscopy measurements (see Fig. S13).

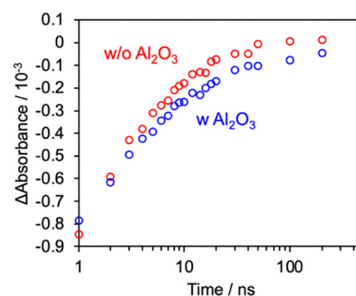


Fig. 3 Time-dependent absorbance changes in *operando* transient absorption measurements of poly-RuRu'/0.15 mM Al₂O₃/NiO (w Al₂O₃) and poly-RuRu'/NiO (w/o Al₂O₃) electrodes, monitored at 465–470 nm. The measurements were conducted in a 50 mM aqueous NaHCO₃ solution under a CO₂ atmosphere (pH 6.6) and under an electrochemical bias of -0.7 V vs. Ag/AgCl.



The transient absorption results indicate that an appropriately thin Al₂O₃ layer formed by modification with a dilute precursor solution effectively suppresses undesirable charge recombination between the semiconductor and the molecular photocatalyst. The resultant enhancement in CO₂ reduction activity is therefore attributable to the suppression of recombination, increasing the availability of photogenerated electrons for CO₂ reduction. By contrast, excessive Al₂O₃ deposition achieved through the use of more concentrated precursor solutions led to a decrease in photoelectrochemical performance.

Consistent with this trend, Guo *et al.* reported that the average electron injection rate from excited Re(I) and Ru(II) bipyridyl complexes into TiO₂ and SnO₂ decreases exponentially with increasing Al₂O₃ overlayer thickness, as revealed by ultrafast transient infrared spectroscopy.¹¹ Guo *et al.* attributed this behavior to the formation of an overly thick insulating layer, which substantially hampered electron transfer. In the present system, a similar trade-off between suppression of back electron transfer and inhibition of forward electron injection is likely operative.

Our results demonstrate that precise control of interfacial electron transfer by tuning the Al₂O₃ precursor concentration prior to dip coating is critical for maximizing the CO₂ reduction performance of NiO photocathodes. However, because electron transfer from the photosensitizing unit to the catalytic unit and back electron transfer from the reduced photosensitizer to the p-type semiconductor occur on comparable timescales (*i.e.*, on the order of microseconds), decoupling these processes experimentally remains challenging. As a result, quantitative evaluation of the back electron transfer rate as a function of the Al₂O₃ precursor concentration has not yet been achieved. To address this limitation, we are currently constructing simplified model systems comprising only the semiconductor and the photosensitizing unit and are carrying out transient absorption measurements to further elucidate the underlying charge-transfer dynamics.

In summary, we have demonstrated that introducing an ultrathin Al₂O₃ interlayer at the interface between a p-type NiO semiconductor and molecular photocatalysts effectively enhances visible-light-driven CO₂ reduction. By systematically tuning the Al₂O₃ precursor concentration, we selectively suppressed charge recombination between NiO and the molecular photocatalyst without substantially impairing electron injection energetics. *Operando* transient absorption spectroscopy revealed that this interfacial modification prolongs the lifetime of the reduced photosensitizing unit, thereby increasing the number of electrons available for CO₂ reduction. Importantly, excessive Al₂O₃ deposition was found to be detrimental, highlighting the critical balance between suppressing back electron transfer and maintaining efficient forward electron transport. These findings provide clear design principles for interfacial engineering in p-type semiconductor/molecular hybrid systems and open new avenues for improving the efficiency of photocathodes for solar-driven CO₂ conversion.

K. Maeda designed/supervised the project and wrote the manuscript draft with Y. T. and M. O. Y. T. conducted most of the experiments with assistance from T. T., J. O., M. T., and M. O. T. T., J. O. and O. I. designed and synthesized the Ru

complexes with Y. T. M. Y., K. Miyata and K. O. performed *operando* FT-IR measurements with Y. T. All authors reviewed the manuscript and approved its submission.

This work was supported by a Grant-in-Aid for Transformative Research Areas (A) “Supra-ceramics” (JP22H05142, JP22H05148, and JP25H01678) and a bilateral collaboration program (JPJSBP120237406) (JSPS). K. O. acknowledges financial support from the JSPS KAKENHI (JP23H01977 and JP23K20039). K. Miyata acknowledges support from the JSPS Transformative Research Areas (B) (JP23H03833).

Conflicts of interest

There are no conflicts to declare.

Data availability

The data supporting this article have been included as part of the supplementary information (SI). Supplementary information is available. See DOI: <https://doi.org/10.1039/d6cc00558f>.

References

- 1 H. Gerischer, *Photochem. Photobiol.*, 1972, **16**, 243–260.
- 2 A. Hagfeldt, G. Boschloo, L. Sun, L. Kloo and H. Pettersson, *Chem. Rev.*, 2010, **110**, 6595–6663.
- 3 M. Watanabe, *Sci. Technol. Adv. Mater.*, 2017, **18**, 705–723.
- 4 A. Nakada, H. Kumagai, M. Robert, O. Ishitani and K. Maeda, *Acc. Mater. Res.*, 2021, **2**, 458–470.
- 5 C. D. Windle, H. Kumagai, M. Higashi, R. Brisse, S. Bold, B. Joussetme, M. Chavarot-Kerlidou, K. Maeda, R. Abe, O. Ishitani and V. Artero, *J. Am. Chem. Soc.*, 2019, **141**, 9593–9602.
- 6 G. Sahara, R. Abe, M. Higashi, T. Morikawa, K. Maeda, Y. Ueda and O. Ishitani, *Chem. Commun.*, 2015, **51**, 10722–10725.
- 7 G. Sahara, H. Kumagai, K. Maeda, N. Kaeffer, V. Artero, M. Higashi, R. Abe and O. Ishitani, *J. Am. Chem. Soc.*, 2016, **138**, 14152–14158.
- 8 Y. Yamazaki, H. Takeda and O. Ishitani, *J. Photochem. Photobiol., C*, 2015, **25**, 106–137.
- 9 E. Palomares, J. N. Clifford, S. A. Haque, T. Lutz and J. R. Durrant, *J. Am. Chem. Soc.*, 2003, **125**, 475–482.
- 10 W. Kim, T. Tachikawa, T. Majima and W. Choi, *J. Phys. Chem. C*, 2009, **113**, 10603–10609.
- 11 J. Guo, C. She and T. Lian, *J. Phys. Chem. C*, 2007, **111**, 8979–8987.
- 12 T.-C. Tien, F.-M. Pan, L.-P. Wang, C.-H. Lee, Y.-L. Tung, S.-Y. Tsai, C. Lin, F.-Y. Tsai and S.-J. Chen, *Nanotechnology*, 2009, **20**, 305201.
- 13 M. Law, L. E. Greene, A. Radenovic, T. Kuykendall, J. Liphardt and P. Yang, *J. Phys. Chem. B*, 2006, **110**, 22652–22663.
- 14 S. Uehara, S. Sumikura, E. Suzuki and S. Mori, *Energy Environ. Sci.*, 2010, **3**, 641–644.
- 15 Z. Bian, T. Tachikawa, S.-C. Cui, M. Fujitsuka and T. Majima, *Chem. Sci.*, 2012, **3**, 370–379.
- 16 G. Natu, Z. Huang, Z. Ji and Y. Wu, *Langmuir*, 2012, **28**, 950–956.
- 17 Z. Ji, M. He, Z. Huang, U. Ozkan and Y. Wu, *J. Am. Chem. Soc.*, 2013, **135**, 11696–11699.
- 18 S. Sumikura, S. Mori, S. Shimizu, H. Usami and E. Suzuki, *J. Photochem. Photobiol., A*, 2008, **199**, 1–7.
- 19 A. Bazyari, Y. Mortazavi, A. A. Khodadadi, L. T. Thompson, R. Tafreshi, A. Zaker and O. T. Ajenifujah, *Appl. Catal., B*, 2016, **180**, 312–323.
- 20 A. A. Bin Mokaizh, J. H. Shariffuddin, A. O. Baarimah, A. Al-Fakih, A. Mohamed, S. O. Baarimah, A. A. Al-Mekhlafi, H. Alenezi, O. A. Olalere and A. A. H. Saeed, *Materials*, 2022, **15**, 3046.
- 21 R. Kamata, H. Kumagai, Y. Yamazaki, M. Higashi, R. Abe and O. Ishitani, *J. Mater. Chem. A*, 2021, **9**, 1517–1529.
- 22 H. Kumagai, G. Sahara, K. Maeda, M. Higashi, R. Abe and O. Ishitani, *Chem. Sci.*, 2017, **8**, 4242–4249.

